Quaternary Research (2018), **90**, 10–25.

doi:10.1017/qua.2018.18

Climate dynamics during the penultimate glacial period recorded in a speleothem from Kanaan Cave, Lebanon (central Levant)

Carole Nehme[a]*, Sophie Verheyden[b], Sebastian F.M. Breitenbach[c], David P. Gillikin[d], Anouk Verheyden[d], Hai Cheng[e,f], R. Lawrence Edwards[e], John Hellstrom[g], Stephen R. Noble[h], Andrew R. Farrant[i], Diana Sahy[i], Thomas Goovaerts[j], Ghada Salem[k], Philippe Claeys[a]

[a]Analytical, Environmental & Geo-Chemistry, Department of Chemistry, Vrije Universiteit Brussel, Brussels, Belgium
[b]Royal Belgian institute of natural sciences, directorate of earth and history of life, Brussels & associate researcher at Vrije Universiteit, Brussel, Belgium
[c]Sediment- & Isotope Geology, Ruhr-Universität, Bochum, Germany
[d]Department of Geology, Union College, 807 Union St, Schenectady, NY 12308, USA
[e]Department of Earth Sciences, University of Minnesota, Minneapolis MN 55455, USA
[f]Institute of Global Environmental Change, Xi'an Jiaotong University, Xi'an, China
[g]Geochemistry Laboratory, Earth Science Department, University of Melbourne, Melbourne, Australia
[h]NERC Isotope Geosciences Laboratory, Keyworth, Nottingham, NG12 5GG, United Kingdom
[i]British Geological Survey, Keyworth, Nottingham, NG12 5GG, United Kingdom
[j]Geological Survey of Belgium, Royal Belgian Institute of Natural Sciences (RBINS), Brussels, Belgium
[k]Association Libanaise d'Etudes speleologiques, Mansourieh El-Matn Lebanon

(Received September 30, 2017; Accepted February 15, 2018)

Abstract

Little is known about terrestrial climate dynamics in the Levant during the penultimate interglacial-glacial period. To decipher the palaeoclimatic history of the Marine Oxygen Isotope Stage (MIS) 6 glacial period, a well-dated stalagmite (~194 to ~154 ka) from Kanaan Cave on the Mediterranean coast in Lebanon was analyzed for its petrography, growth history, and stable isotope geochemistry. A resolved climate record has been recovered from this precisely U–Th dated speleothem, spanning the late MIS 7 and early MIS 6 at low resolution and the mid–MIS 6 at higher resolution. The stalagmite grew discontinuously from ~194 to ~163 ka. More consistent growth and higher growth rates between ~163 and ~154 ka are most probably linked to increased water recharge and thus more humid conditions. More distinct layering in the upper part of the speleothem suggests strong seasonality from ~163 ka to ~154 ka. Short-term oxygen and carbon isotope excursions were found between ~155 and ~163 ka. The inferred Kanaan Cave humid intervals during the mid–MIS 6 follow variations of pollen records in the Mediterranean basins and correlate well with the synthetic Greenland record and East Asian summer monsoon interstadial periods, indicating short warm/wet periods similar to the Dansgaard-Oeschger events during MIS 4–3 in the eastern Mediterranean region.

Keywords: Penultimate glacial; Stable isotopes; Lebanon; Speleothem; Millennial-scale oscillations

INTRODUCTION

Climate records spanning the last 400,000 yr (Dansgaard et al., 1993; Martrat et al., 2007; Wang et al., 2008) have shown that glacial–interglacial (G-IG) cycles are not simple repeating patterns (Martrat et al., 2007; Past Interglacials Working Group of PAGES, 2016). Each cycle experienced a unique set of climatic boundary conditions based on variations in orbital parameters, including the earth's eccentricity, axial tilt, and precession. Therefore, the resulting orbital-scale variations are far from being identical from one G-IG cycle to the next (Margari et al., 2010; Wainer et al., 2013). In addition, differences in the magnitude of forcing factors such as ice rafted debris discharge and solar radiation influence the amplitude of global atmospheric and sea surface temperatures (SSTs), as well as the amplitude, number, and duration of stadial/interstadial periods during each G-IG cycle.

Millennial-scale climatic variations during the last glacial cycle are extensively documented in ice cores (Dansgaard, 1964; Blunier and Brook, 2001; Rohling et al., 2003; North Greenland Ice Core Project, 2004; Capron et al., 2010; Wolff et al., 2010; Rasmussen et al., 2014), from marine records (Goñi et al, 2000; Peterson at al., 2000; de Abreu et al., 2003; Siddal et al., 2003; Jouzel et al., 2007; Martrat et al., 2007; Margari et al., 2010), and in terrestrial deposits (Fletcher and Sánchez Goñi, 2008; Wang et al.,

*Corresponding author at: Laboratoire UMR IDEES 6266 CNRS, 7, Rue Thomas Becket 76280, Mont Saint-Aignan, France. E-mail address: carole.nehme@univ-rouen.fr (C. Nehme).

2008; Tzedakis et al., 2009; Fletcher et al., 2010; Cheng et al., 2012; Genty et al., 2013; Ünal-İmer et al., 2015). Much less is known about millennial-scale variability in older glacial cycles such as the penultimate glacial period, between 135 and 185 ka (Ehlers and Gibbard, 2007) – equivalent to Marine Oxygen Isotope Stage 6 (MIS 6). With a lack of Northern Hemisphere ice core records covering the MIS 6 period, some marine (Margari et al., 2010, 2014) and terrestrial records (Wang et al., 2008; Cheng et al., 2012) provide alternative paleoclimate records, along with the synthetic Greenland temperature proxy profile (Barker et al., 2011).

For the last glacial cycle, the well-dated Hulu-Sanbao cave records in China (Wang et al., 2008; Cheng et al., 2012) revealed enhanced monsoonal activity occurring synchronously with the Greenland Dansgaard-Oeschger (D-O) warming events. Speleothems from Villars Cave, France (Genty et al., 2003), recorded similar millennial-scale patterns interpreted as warm and/or wet peaks. The occurrence of comparable millennial-scale variability in the Hulu-Sanbao and Villars Cave speleothem records (Wainer et al., 2013) suggests that D-O–like millennial-scale climate fluctuations also occurred during the penultimate glacial period, albeit with different patterns, intensities, and duration compared with MIS 3.

In Europe, D-O–like patterns during the penultimate glaciation were reflected in the isotope patterns from Villars Cave, France (Wainer et al., 2013), the Tana Che Urla Cave speleothems records, central Italy (Regattieri et al., 2014), and the Abaliget Cave speleothem records, southern Hungary (Koltai et al., 2017). Pollen and $\delta^{18}O_{plank.}$ marine records from the Portuguese MD01-2444 core (Margari et al., 2010, 2014) also suggest warmer conditions during early MIS 6 (de Abreu et al., 2003), with less prominent millennial-scale variability. D-O–like climatic oscillations are also recorded in the marine $SST_{alk.}$ record from the Iberian margin ODP-977 core (Martrat et al., 2007), with more than nine cold and warm events during early and mid-MIS 6 (ca. 150–178 ka, according to Margari et al., 2010). These identified climatic oscillations, triggered in response to global climatic warming, were not restricted to oceanic processes linked to deglaciation but also included shifts in atmospheric circulation (Stocker and Johnsen, 2003; Barker et al., 2009) that imprinted terrestrial records. Teleconnections of these stadial–interstadial changes across both Northern Hemisphere (Wang et al., 2001; Fleitmann et al., 2009) and mid- to low-latitude regions (Wang et al., 2008; Cheng et al., 2012; Ünal-İmer et al, 2015) are well established, partially thanks to speleothem records with their ability to constrain precisely the timing of these dynamics. However, understanding millennial-scale variability (Jouzel et al., 2007) beyond the last G-IG cycle, such as for the penultimate glacial period, ca. 135–185 ka, is still hampered by the scarcity of continuous low- to midlatitude terrestrial records with robust chronologies and sufficiently high resolution.

Speleothems are terrestrial archives that can provide high-resolution proxy time series for paleoclimate reconstruction data with sufficient precision to date the timing of climatic changes (Genty et al., 2003; Cheng et al., 2012). In the eastern Mediterranean basin, MIS 6 and 7 were both the subject of marine (Emeis et al., 2003; Ziegler et al., 2010), lacustrine (Tzedakis et al., 2004; Tzedakis et al., 2009; Roucoux et al., 2008, 2011; Litt et al., 2014; Gasse et al., 2015), and speleothem (Ayalon et al., 2002; Bar-Matthews et al., 2003; Bar-Matthews, 2014) paleoclimate studies. These studies demonstrate warmer and overall wetter conditions than previously thought for MIS 6 (Chedadi and Rossignol-Strick, 1995), concurrent with glacial conditions in northern latitude regions (Ehlers et al., 2011). In fact, the penultimate glacial period corresponds to the late Saalian glaciation in Europe (Ehlers and Gibbard, 2007) but was not a "typical" glacial period. Characteristic of this atypical nature is the deposition of sapropel S6 in the eastern Mediterranean (Bard et al., 2002; Emeis et al., 2003; Ziegler et al., 2010). Although most of the Mediterranean sapropel occurs generally during interglacial periods, the S6 occurred during a glacial period. The S6 deposition around 165–179 ka resulted from an enhanced low-latitude hydrologic activity through an intensified monsoon activity in eastern Africa, associated with an insolation maxima and a strong precession minima that led to a northward migration of the Intertropical Convergence Zone (Rossignol-Strick and Paterne, 1999).

On the surrounding landmasses, climate variations during MIS 6 showed a similar response to both regional and global forcing. Climatic variations on the continent were, however, distinctive in amplitude and rhythmicity, emphasized by topographic settings, steep temperature, and rainfall gradients across the Levant. The Yammouneh Lake records from Lebanon showed dry and cold climate conditions at the MIS 7/6 transition (Gasse et al., 2015), followed by more humid conditions and increased rainfall during the deposition of sapropel S6. Wet events during early and mid–MIS 6 were also recorded in the Peqiin and Soreq speleothem records (Ayalon et al., 2002) and in the Negev region (Vaks et al., 2006), during a generally cold but still humid period in the southern Levant. The Lake Van records (eastern Turkey) were less strongly influenced by the environmental conditions that led to sapropel deposition in the Mediterranean but show millennial climate variability intercalated by warm/wet conditions during the early MIS 6 (Stockhecke et al., 2014). Climatic oscillations with low-amplitude variations were also detected in the Ionian (Roucoux et al., 2008, 2011) and Tenaghi-Philippon (Tzedakis et al., 2004) pollen profiles and demonstrate the significant downstream impact of North Atlantic millennial-scale climate variability on the hydrology and vegetation in northwestern Greece during MIS 6.

Although several records in northern and southern Europe demonstrated North Atlantic millennial-scale oscillations during MIS 6, only a few high-resolution records show a similar climatic pattern in the eastern Mediterranean for this time period. To expand our understanding of this critical time window in the eastern Mediterranean, the petrography, growth history, and stable isotope geochemistry of a speleothem from the northern Levant (Lebanon) was examined. Stalagmite K2-2010 from Kanaan Cave, located close to the Mediterranean coast, provides a precise U–Th dated and highly resolved terrestrial record of the climate history from the northern Levant.

https://doi.org/10.1017/qua.2018.18 Published online by Cambridge University Press

This record spans the late penultimate interglacial period (MIS 7a) and the early penultimate glacial period (MIS 6) at low resolution, and the mid–penultimate glacial period (mid-MIS 6) at high resolution. The new isotope time series is used to compare the climate variability in the northern Levant with high-resolution records from the eastern and western Mediterranean and to gain insight into the major climatic teleconnection patterns and forcing factors of that period.

SITE AND SAMPLE DESCRIPTION

The Kanaan Cave site and climatic setting

Kanaan Cave (33°54.4167 N, 35°36.4167 E) is located on the western flank of central Mount Lebanon, 15 km northeast of Beirut, Lebanon (Fig. 1). Situated only 2.5 km from the Mediterranean coast at an elevation of 98 meters above sea level (m asl), the site has a "maritime influenced" temperate Mediterranean climate (Csa climate in the Köppen-Geiger classification; Peel et al., 2007). The climate is seasonal, with wet winters (November to February) and dry, hot summers (from May to October) and an annual precipitation typically between 880 and 1100 mm (The World Bank, 2003). The present climate is influenced by the Atlantic westerlies, which bring in moist winds associated with extratropical cyclones. These originate in the Atlantic and track east across the Mediterranean Sea, forming a series of subsynoptic low-pressure systems. In winter, outbreaks of cold air plunging south over the relatively warm Mediterranean enhance cyclogenesis and create the Cyprus Low. These low-pressure systems drive moist air onshore, generating intense orographic rainfall across the mountains of the northern Levant. The duration, intensity, and track of these storm systems strongly influence the amount of rainfall in this region.

The Kanaan Cave is a 162 m long relict conduit discovered during quarrying in 1997. It is developed in the Middle Jurassic Kesrouane Formation, a limestone unit with an average stratigraphic thickness of 1000 m (Dubertret, 1975). Stalagmite K2-2010 was growing on rimstone dams covering clay sediments in the central part of the Collapse I chamber (Nehme et al., 2013) and at 20 m from the cave entrance (which did not exist prior to 1997). The passage height at this location is 0.5 m with approximately 50 m of limestone overburden. At the time of collection, the stalagmite received no drip water, although some drip water occurs in other parts of the Collapse I chamber during winter and spring seasons. The cave is generally dry during the summer months. The air temperature in Collapse I chamber is 19 ± 0.5°C during the autumn season.

Petrographic description of sample K2-2010

The speleothem K2-2010 is 21 cm long and up to 7 cm in diameter (Fig. 2). In cross section, it displays regular layers of dense calcite with thin (<0.1 mm) laminations in some sections. The speleothem has three clearly defined petrographic segments with different crystal fabrics along its growth axis.

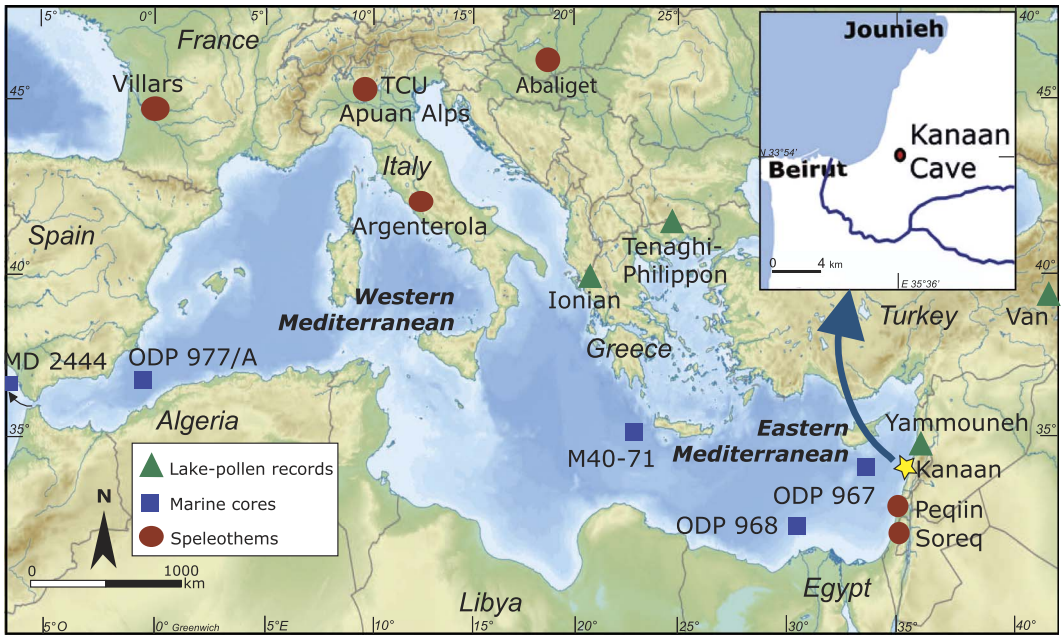

Figure 1. (color online) Location of Kanaan Cave and other Mediterranean palaeoclimatic records spanning Marine Oxygen Isotope Stage (MIS) 6 and MIS 7. Speleothems: Villars Cave (Wainer at al., 2011, 2013), Apuan Alps–Tana Che Urla (TCU) Cave (Regattieri et al., 2014), Abaliget Cave (Koltai et al., 2017), Argenterola Cave (Bard et al., 2002), Peqiin Cave (Bar-Matthews et al., 2003), and Soreq Cave (Ayalon et al., 2002). Lacustrine records: the Yammouneh paleolake (Gasse et al., 2015), Lake Van (Litt et al., 2014), and the Ionian (Roucoux et al., 2008, 2011) and Tenaghi-Philippon (Tzedakis et al., 2004) paleo lakes. Marine cores: M40-71 (Emeis et al., 2003), ODP 968 (Ziegler et al., 2010), ODP 967 (Rossignol-Strick, 1995; Emeis et al., 2003; Scrivner et al., 2004), ODP 977/A (Martrat et al., 2004, 2007), and MD-2444 (Margari et al., 2010, 2014).

https://doi.org/10.1017/qua.2018.18 Published online by Cambridge University Press

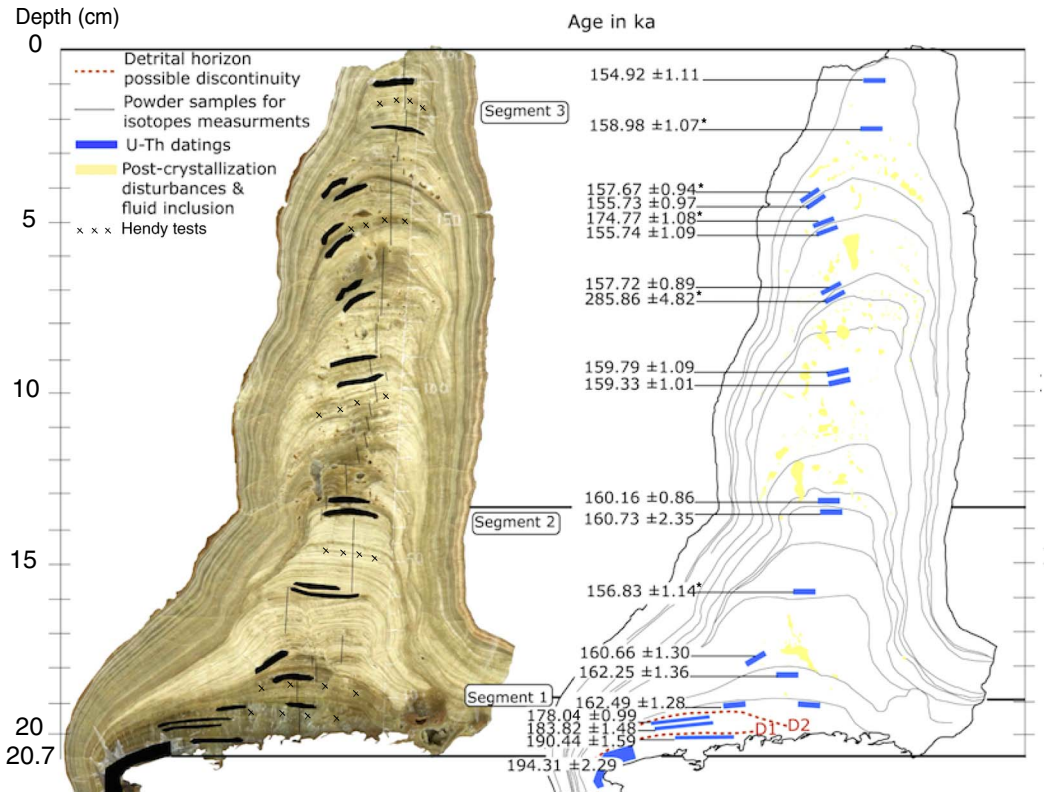

Figure 2. (color online) Scan and sketch of speleothem K2-2010 showing the position of the powder samples for isotope measurements and uranium-series dating. The dashed line in segment 1 indicates a possible discontinuity; segment 2 is characterized by a candle-like shape and shows laminae fabrics, not seen in segment 1. Segment 3 shows varying diameters, many fluid inclusions, and postcrystallization disturbances in an alternating laminated texture of white porous and dark compact layers. Ages with asterisk (*) were excluded from the model age.

The basal segment (segment 1) is 1.5 cm thick (Fig. 2) and comprises uniform translucent carbonate with a columnar fabric (Frisia, 2015), considered closer to isotopic equilibrium. A thin clay layer occurs 19.9 cm below the top of the stalagmite. The middle segment (segment 2) is 5.8 cm thick and displays a translucent columnar microcrystalline fabric from 17.8 to 18.8 cm from the top. Between 13 and 17.8 cm from the top, this turns into a laminated fabric with white porous layers. The topmost segment (segment 3) is 13 cm long, with a general structure characterized by alternating couplets (Genty and Deflandre, 1998; Fairchild and Baker, 2012) of white porous and compact dark layers. In some parts of the segment, mainly at 8 to 9 cm and 5 to 5.5 cm depth, the white porous layers of the couplets are thicker and interrupted by postcrystallization disturbances. In other parts of segment 3, mainly from 11.2 to 13 cm, 5.6 to 6.8 cm, and at 5 and 3.8 cm, the dark compact layers are denser. Some pores were observed at several levels within segment 3. The base of the speleothem has a diameter of 7 cm, which decreases to 1.6 cm at the top.

METHODS

U–Th isotope measurement

Stalagmite K2-2010 was cut along its growth axis and polished using 120–4000 µm silicon carbide sandpaper. Petrographic observations were performed with an optical binocular microscope. Two preliminary U-series dates were obtained at the National Isotope Geosciences Laboratory (NIGL), British Geological Survey, Keyworth (United Kingdom), and at the Geochemistry Laboratory, Earth Science Department, University of Melbourne, Australia, respectively. Subsequently, 18 ages were determined at the University of Minnesota (USA), using the procedures for uranium and thorium chemical separation and purification described in Edwards et al. (1987) and Cheng et al. (2013; 2016). One hundred to 400 mg powdered calcite samples were collected with a dental drill from 17 levels along the growth axis of the speleothem, taking care to sample along growth horizons. Minnesota and NIGL data were obtained on Thermo Neptune Plus multicollector inductively coupled plasma mass spectrometers (MC-ICP-MSs) following procedures modified from Cheng et al. (2013) at Minnesota and Heiss et al. (2012) and Smith et al. (2016) at NIGL. Melbourne data were obtained on a Nu Instruments MC-ICP-MS using an internally standardized parallel ion-counter procedure and calibrated against the HU-1 secular equilibrium standard following the procedures of Hellstrom (2003). Correction for detrital Th content was applied using initial activity ratios of detrital thorium $(^{230}Th/^{232}Th)_i$ of 0.93 ± 0.73. These values and their relative 2σ uncertainty were calculated using a Monte Carlo "stratigraphic constraint" procedure based on the series of U/Th ages

https://doi.org/10.1017/qua.2018.18 Published online by Cambridge University Press

(Hellstrom, 2006) and compatible with the approach of Roy-Barman and Pons-Branchu (2016). Under this method, the $(^{230}Th/^{232}Th)_i$ and its uncertainty are optimized in order to bring all ages into correct stratigraphic order within their age uncertainties. Ages are calculated from time of analysis (2016) and reported in thousand years before present (ka BP) relative to AD 1950, with an uncertainty at the 2σ level, typically between 500 and 1000 yr (see Table 1). The age model was constructed using the Constructing Proxy Records from Age models (COPRA) routine (Breitenbach et al., 2012), based on polynomial interpolation and 5000 Monte Carlo simulations.

Calcite and water stable isotope measurement

Samples for $\delta^{13}C$ and $\delta^{18}O$ measurements were drilled along the speleothem central axis with a Merchantek Micromill. Between every sample, the drill bit and sampling surface were blown clean with compressed air. Sampling resolution in K2-2010 was 250 μm. A total of 800 samples and 80 duplicate samples (92% replicability) were analyzed using either a Nu Carb carbonate device coupled to a Nu Perspective MS at the Vrije Universiteit Brussel or a Thermo Gas Bench II connected to a Thermo Delta Advantage mass spectrometer in continuous flow mode at Union College (USA). Analytical uncertainties were better than 0.1 ‰ (1σ) for oxygen and 0.05 ‰ (1σ) for carbon on both instruments. All $\delta^{18}O$ and $\delta^{13}C$ values are calibrated against the international standard and are reported in per mil (‰) relative to Vienna Pee Dee belemnite. The stalagmite was tested for isotopic equilibrium conditions using recent calcite samples collected in the cave and Hendy tests (Hendy, 1971), carried out at six different levels along the speleothem growth axis (Table 2).

Six seepage and pool water samples from Kanaan Cave were collected in the autumn–winter season for $\delta^{18}O$ and δD measurements in hermetically sealed glass bottles. Isotope measurements were performed at the Vrije Universiteit Brussel on a Picarro L2130-i analyzer using the cavity ring–down spectroscopy (CRDS) technique (Van Geldern and Barth Johannes, 2012). All values are reported in per mil (‰) relative to Vienna standard mean ocean water. Analytical uncertainties (1σ) were better than 1‰ for δD and 0.1‰ for $\delta^{18}O$.

RESULTS

Chronology

Twenty uranium series dates were obtained from stalagmite K2-2010 (Table 1). The age distribution indicates that K2-2010 grew discontinuously from ca. 194.3 ± 2.3 ka to 154.3 ± 1.2 ka (COPRA age model). In the basal part, two discontinuities, characterized by thin clay layers occur at 20 cm (D1) and 19.3 cm (D2) depth. These hiatuses are estimated to have occurred from 190.2 to 183.3 ka and from 175.3 to 162.7 ka (interpolated ages) (Fig. 3). After 162.7 ka (during the glacial maximum), the stalagmite growth is more continuous.

Age uncertainties are greatest for dates obtained from the lowermost part of the speleothem where segments 1 and 2 (Fig. 2) are in close proximity to the clay horizon on which the speleothem grew, as reflected in their relatively low $^{230}Th/^{232}Th$ values. The stratigraphic uncertainties are less than 1 mm (i.e., between 0.8 ka and 1.4 ka) for all dates except for the basal age of 194.3 ± 2.3 (2σ), which shows a stratigraphic uncertainty of 2 mm (~2.1 ka). Several dates are not in stratigraphic order (i.e., samples, 8, 10, 12, 16, and 13; Table 1). Most of these samples are located in porous areas of the speleothem. These porous regions may have experienced U–Th open-system behavior (Richards and Dorale, 2003; Borsato et al., 2005) via dissolution and recrystallization processes of the primary carbonate (Frisia, 2015) with attendant uranium loss (Ortega et al., 2005; Hoffmann et al., 2009; Lachniet et al., 2012), remobilization, or postdepositional filling of pores (Schwarcz, 1989) resulting in out-of-sequence ages. These samples were considered as geologically induced age outliers and excluded from the age model. On the other hand, two couples of U–Th dates (e.g., coupled dates 14 and 15; 1 and 2) have overlapping uncertainties at the 2σ level, both of which were included in the age model.

The age model is based on a polynomial interpolation for each of the three segments of the stalagmite. For the basal segments of the stalagmite, dated between ~194 and ~163 ka and including at least two long hiatuses, interpolation between the available four dates was used to construct the age model, allowing an estimation of an extremely low growth rate from ~194 to 190 ka and ~183 to 175 ka, with at least one hiatus (Fig. 3). The overall finding is that there are very likely multiple hiatuses, which cannot be resolved with four dates. The age model of the basal part of the stalagmite is therefore regarded as only approximate. In the upper part, dated between ~163 and ~155 ka, the interpolation was performed between 11 ages (Fig. 3), permitting calculation of continuous growth rate changes without any drastic inflections in the age-depth plot. The polynomial function assumes that all dates should be traversed (within errors) and generates a monotonously positive depth-age slope (Breitenbach et al., 2012). The median and 2.5% and 97.5% confidence intervals are based on 5000 Monte Carlo simulations. COPRA handles multiple hiatuses, as long as each is bracketed by at least two dates, which is the case in this sample.

Oxygen and carbon isotope variations

If carbonate precipitation occurs at or near isotopic equilibrium, the calcite $\delta^{18}O$ values should not show any significant enrichment along a single lamina away from the growth axis and no covariation between $\delta^{18}O$ and $\delta^{13}C$ values should occur (Hendy, 1971). Hendy tests performed along six different growth layers (Fig. 2) show less than 1‰ variation for $\delta^{18}O$ values and less than 0.5‰ for $\delta^{13}C$ values

https://doi.org/10.1017/qua.2018.18 Published online by Cambridge University Press

Table 1. Corrected U/Th ages for the Kanaan K2-2010 stalagmite with uncertainties given in 2σ level. U–Th isotope data are expressed as activity ratios. U decay constants: $\lambda_{238} = 1.55125 \times 10^{-10}$ (Jaffey et al., 1971); $\lambda_{234} = 2.82206 \times 10^{-6}$ (Cheng et al., 2013). Th decay constant: $\lambda_{230} = 9.1705 \times 10^{-6}$ (Cheng et al., 2013). Corrected $^{230}Th/^{234}U$ ages calculated using an initial $^{230}Th/^{232}Th$ activity ratio of 0.93 ± 0.73 corresponding to an atomic ratio of $5.0 \pm 3.9 \times 10^{-6}$. Data with asterisk (*) are outliers and not used to construct the age model.

Lab ID	Sample ID	Depth (mm)	^{238}U (ng/g)	$(^{230}Th/^{232}Th)$	$(^{230}Th/^{238}U)$	$(^{234}U/^{238}U)$	$(^{232}Th/^{238}U) \times 10^3$	$\delta^{234}U^a$ (measured)	$\delta^{234}U^b$ (initial)	^{230}Th age (ka) (uncorrected)	^{230}Th age (ka) (corrected)	^{230}Th age (ka BP) (corrected)
84-21	06	8	310.0	446.5	0.7902 ± 0.0024	1.035 ± 0.001	1.770 ± 0.018	34.5 ± 1.1	56 ± 1	155.17 ± 1.12	154.99 ± 1.11	154.92 ± 1.11
SV-16*	16*	22	260.7	2052.2	0.7993 ± 0.0018	1.035 ± 0.002	0.389 ± 0.004	34.6 ± 1.7	54 ± 3	159.07 ± 1.07	159.04 ± 1.07	158.98 ± 1.07*
SV-12*	12*	36	249.2	340.6	0.7998 ± 0.0015	1.038 ± 0.002	2.348 ± 0.024	37.9 ± 1.6	59 ± 2	157.96 ± 0.91	157.74 ± 0.94	157.67 ± 0.94*
SV-11	11	39	269.0	308.2	0.7955 ± 0.0015	1.038 ± 0.002	2.581 ± 0.026	38.1 ± 1.7	59 ± 3	156.05 ± 0.95	155.80 ± 0.97	155.73 ± 0.97
SV-10*	10*	48	167.6	262.4	0.8286 ± 0.0013	1.030 ± 0.002	3.158 ± 0.032	30.2 ± 1.6	49 ± 3	175.13 ± 1.06	174.83 ± 1.08	174.77 ± 1.08*
SV-05	05	52	270.8	486.4	0.7940 ± 0.0017	1.037 ± 0.002	1.632 ± 0.017	36.6 ± 2.0	57 ± 3	155.97 ± 1.09	155.81 ± 1.09	155.74 ± 1.09
SV-09	09	67	334.5	295.6	0.7984 ± 0.0014	1.036 ± 0.002	2.701 ± 0.027	36.2 ± 1.5	57 ± 2	158.04 ± 0.88	157.78 ± 0.89	157.72 ± 0.89
SV-08*	08*	70	934.1	1021.5	0.9383 ± 0.0025	1.009 ± 0.002	0.919 ± 0.010	9.0 ± 1.7	20 ± 4	285.97 ± 4.77	285.92 ± 4.82	285.86 ± 4.82*
SV-15	15	89	277.4	360.1	0.8014 ± 0.0019	1.034 ± 0.002	2.225 ± 0.023	34.5 ± 1.6	54 ± 3	160.07 ± 1.08	159.86 ± 1.09	159.79 ± 1.09
SV-14	14	96	267.0	451.8	0.8004 ± 0.0017	1.035 ± 0.002	1.771 ± 0.018	34.6 ± 1.6	54 ± 3	159.56 ± 1.00	159.39 ± 1.01	159.33 ± 1.01
SV-04	04	132	366.8	165.9	0.8035 ± 0.0012	1.035 ± 0.001	4.842 ± 0.049	35.3 ± 1.3	56 ± 2	160.69 ± 0.77	160.22 ± 0.86	160.16 ± 0.86
SV-03	03	136	293.8	28.9	0.8069 ± 0.0014	1.032 ± 0.002	27.88 ± 0.283	32.4 ± 1.5	51 ± 2	163.51 ± 0.91	160.79 ± 2.35	160.73 ± 2.35
SV-13*	13*	159	368.4	185.8	0.7929 ± 0.0019	1.032 ± 0.002	4.268 ± 0.044	32.0 ± 1.8	50 ± 3	157.31 ± 1.09	156.89 ± 1.14	156.83 ± 1.14*
SV-02	02	175	209.4	121.6	0.8072 ± 0.0019	1.038 ± 0.002	6.640 ± 0.068	37.7 ± 2.0	59 ± 3	161.37 ± 1.18	160.73 ± 1.30	160.66 ± 1.30
SV-01	01	184	359.9	163.2	0.8082 ± 0.0022	1.035 ± 0.002	4.953 ± 0.051	35.4 ± 2.0	56 ± 3	162.78 ± 1.32	162.32 ± 1.36	162.25 ± 1.36
SV-07	07	191	213.5	144.7	0.7926 ± 0.0021	1.018 ± 0.002	5.478 ± 0.057	18.0 ± 1.6	28 ± 3	163.09 ± 1.21	162.55 ± 1.28	162.49 ± 1.28
SV-17	17	196	176.6	210.1	0.8073 ± 0.0012	1.002 ± 0.001	3.842 ± 0.039	1.9 ± 1.2	3 ± 2	178.49 ± 0.93	178.11 ± 0.99	178.04 ± 0.99
SV-18	18	198	162.4	93.8	0.8173 ± 0.0019	1.001 ± 0.001	8.711 ± 0.089	1.0 ± 1.1	2 ± 2	184.77 ± 1.32	183.88 ± 1.48	183.82 ± 1.48
SV-0	0	201	169.6	75.2	0.8312 ± 0.0015	1.004 ± 0.002	11.05 ± 0.112	3.7 ± 1.5	6 ± 3	191.62 ± 1.34	190.50 ± 1.59	190.44 ± 1.59
120325-211	00	203	136.0	47.7	0.8230 ± 0.0024	0.991 ± 0.003	3.209 ± 0.017	9.1 ± 2.5	16 ± 5	194.71 ± 2.28	194.37 ± 2.29	194.31 ± 2.29

[a] $\delta^{234}U = ([^{234}U/^{238}U]\ \text{activity} - 1) \times 1000$.
[b] $\delta^{234}U_{initial}$ was calculated based on ^{230}Th age (T) (i.e., $\delta^{234}U_{initial} = \delta^{234}U_{measured} \times e\lambda_{234} \times T$).

Table 2. Hendy tests conducted on six levels from top (HB) to bottom (HG) using four to five samples on a single lamina for each level.

	Oxygen $\delta^{18}O$				Carbon $\delta^{13}C$			
Level	Average	Minimal	Maximal	Standard deviation	Average	Minimal	Maximal	Standard deviation
HB	–3.77	–3.86	–3.66	0.07	–10.45	–10.66	–10.15	0.17
HC	–3.38	–4.16	–3.06	0.46	–9.26	–9.73	–9.09	0.27
HD	–6.05	–6.25	–5.93	0.12	–11.05	–11.33	–10.92	0.16
HE	–4.76	–4.80	–4.70	0.04	–10.76	–10.99	–10.61	0.14
HF	–4.86	–4.99	–4.73	0.12	–10.79	–10.60	–10.60	0.21
HG	–4.42	–4.47	–4.32	0.06	–10.80	–10.95	–10.45	0.21

along the tested laminae (Table 2). Therefore, no indication of out-of-equilibrium deposition was detected in the central part of the stalagmite (apex), which is where the samples for isotope analysis were collected from.

The $\delta^{18}O$ values from K2-2010 (Fig. 4) range from –2.9‰ to –6.6‰, with an overall mean of –4.7 ‰. Four distinct peaks in $\delta^{18}O$ values can be identified: at 3 cm (peak I), 5 cm (peak II), 13 cm (peak III), and 19.4 cm (peak IV) depth. The $\delta^{13}C$ values range from –8.1‰ to –12.2‰ around a mean of 10.6‰. Based on the $\delta^{18}O$ variations, the stalagmite can clearly be divided in a basal part (segment 1) with overall $\delta^{18}O$ values of approximately –4.4‰, but lower $\delta^{18}O$ values of –4.0‰ to –6.6‰ in the upper part. In segment 2, a positive shift of ~ 3‰ occurred around 19 cm from top, visible in the $\delta^{13}C$ record, albeit less pronounced in the $\delta^{18}O$ record. Both $\delta^{18}O$ and $\delta^{13}C$ begin to decrease between 19 and 13 cm depth, with a decrease to –3.6‰ (mean value) for $\delta^{18}O$ and –10.2‰ (average value) for $\delta^{13}C$. The $\delta^{13}C$ shift occurs simultaneously with a decrease in stalagmite diameter. Higher $\delta^{18}O$ and $\delta^{13}C$ values are rather stable compared with the isotopic values in segment 1, but the stalagmite diameter decreases slowly from the bottom to the top of segment 2.

At about 13 cm depth (Segment 3), a second shift in $\delta^{18}O$ (3‰ amplitude) and $\delta^{13}C$ (2.5‰ amplitude) values occurred simultaneously (peak III) with an abrupt increase in stalagmite diameter and a change in petrographic fabric (Fig. 4). However, other changes in diameter do not occur simultaneously with changes in isotopic values as demonstrated within segment 2 (Fig. 4). From 13 to 10 cm depth (basal part of segment 3), $\delta^{18}O$ values vary between –5.0‰ and –6‰, and $\delta^{13}C$ values decrease from approximately –10.5‰ to approximately –12‰. Whereas $\delta^{13}C$ values remained unchanged onward from 10 cm depth to the top (mean approximately –10.7‰), $\delta^{18}O$ values showed two rapid significant negative excursions, located respectively at 5 cm (peak II) and 3 cm (peak I) depth. Peak I shows low $\delta^{18}O$ values, reaching –6.5‰. The stalagmite diameter in segment 3 follows the $\delta^{18}O$ value variability pattern. The diameter is larger at peaks I, II, and III (Fig. 4) and decreases with higher $\delta^{18}O$ values.

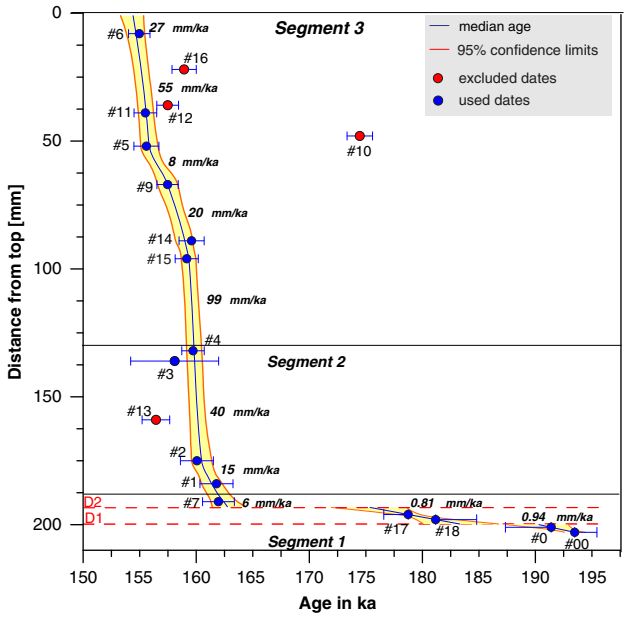

Figure 3. (color online) Age model of Kanaan record: growth rate of the stalagmite with respect to distance (in millimeters) from the top, using COPRA polynomial statistics model between two consecutive dates.

DISCUSSION

Integrated climatic interpretation of the speleothem proxies

Speleothem growth rate has three significant determinants: (1) calcite saturation (Ca^{2+} and HCO_3^- concentrations), (2) CO_2 degassing, and (3) temperature and water supply rate (Dreybrodt, 1988; Baker et al., 1998; Genty et al., 2001). The water supply rate indirectly depends on the amount of rainwater. Ca-ion concentration depends on host rock dissolution processes governed by soil CO_2 concentration. Soil CO_2 concentration activity is mainly a function of precipitation (or evapostranspiration) and temperature that would control the biological activity in the soil. In a Mediterranean climate, the precipitation could be more important than temperature as the precipitation amount could be the limiting factor for biological activity. Therefore, warm and humid conditions are generally seen as ideal for speleothem deposition. Cave ventilation, as well as in-cave pCO_2 dynamics will govern precipitation processes (Dreybrodt, 1988; Baker and Smart, 1995; Genty et al., 2006; Breitenbach et al., 2015).

Speleothem diameter can also be used to infer climatic conditions because it is strongly related to the water supply,

https://doi.org/10.1017/qua.2018.18 Published online by Cambridge University Press

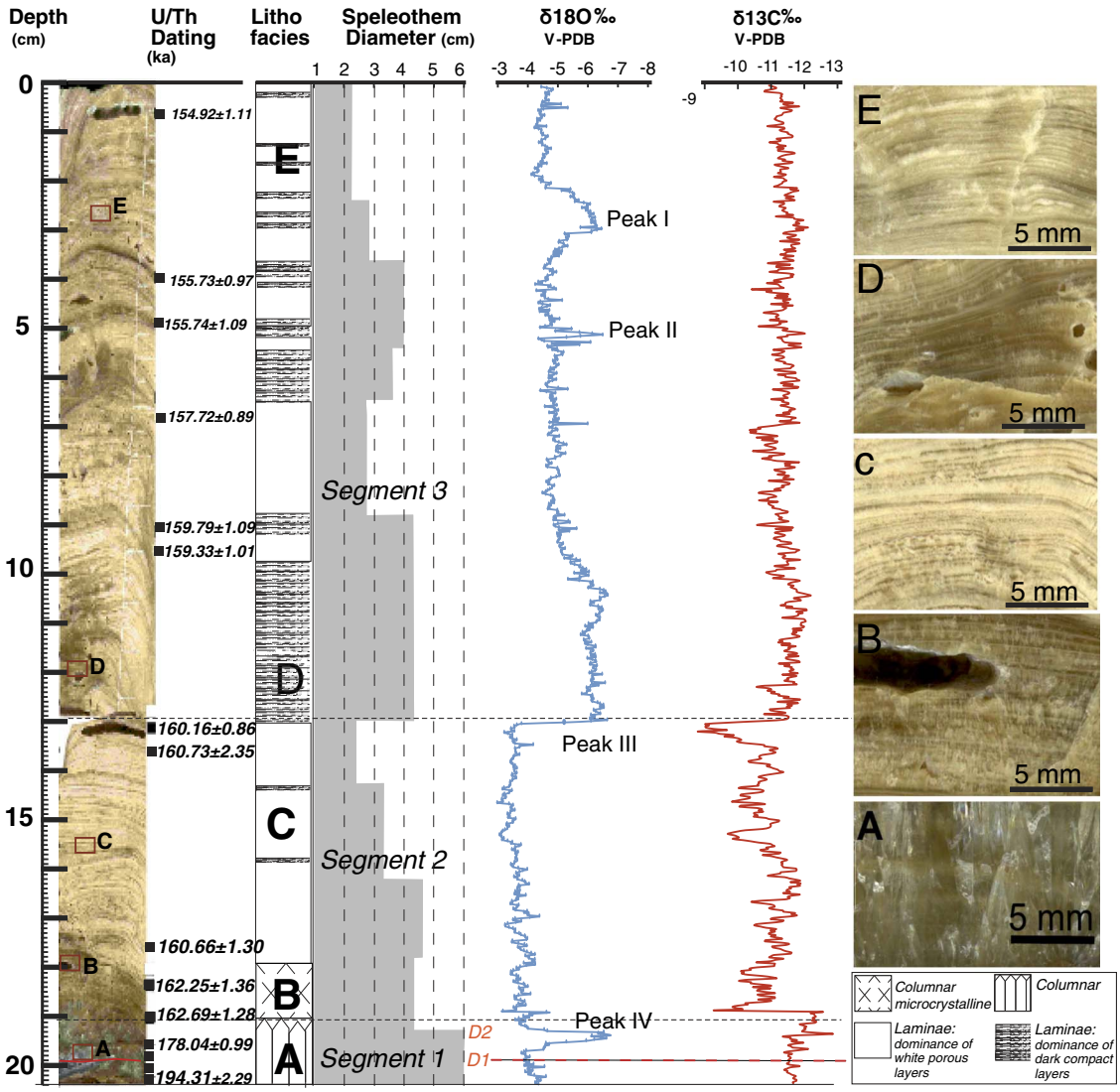

Figure 4. Stratigraphic log of the speleothem K2-2010 showing from left to right: an image scan of the speleothem in the center of the growth axis, the location of the U–Th dating, the lithofacies describing the structure of the calcite fabric, the diameter of the speleothem, and the $\delta^{18}O$ and $\delta^{13}C$ isotopic data. The red boxes on the left side of the figure show the locations of the photographs (A, B, C, D, and E) on the right side. (A) Columnar fabric. (B) Columnar microcrystalline fabric. (C) Abundance of white porous laminae. (D) Abundance dark compact laminae with fluid inclusion pores. (E) Alternating couplets of white porous and compact dark layers. V-PDB, Vienna Pee Dee belemnite. (For interpretation of the references to color in this figure legend, the reader is referred to the web version of this article.)

drip water flow, and thus the effective precipitation (Dreybrodt, 1988, 1999) leading us to generally relate maximal diameter to wetter periods and minimal diameter to drier periods. Calcite fabrics in speleothems develop under certain environmental conditions. The most important parameters are fluid flow, which is directly dependent on drip rates and the presence of impurities that influence a determined spatial arrangement of crystal habit with dominant forms (Frisia, 2015). The sudden change in crystal habit could be related to rapid shifting in the dripping conditions and behavior such as a change from a homogenous drip rate to irregular with seasonal change (Muñoz-García et al., 2016).

Generally, variations in $\delta^{13}C$ values can be the result of several factors: soil biogenic CO_2, a mix between C3/C4 vegetation, reduced or increased soil vegetation, increased residence time and carbonate dissolution, change in soil respiration rate, and/or seasonality. In the eastern Mediterranean, $\delta^{13}C_{calcite}$ variations are mainly linked to changes in soil biogenic CO_2 through changes in local effective hydrologic conditions (Bar-Matthews et al., 1999, 2003; Frumkin et al., 2000; Verheyden et al., 2008; Cheng et al., 2015). The $\delta^{18}O_{calcite}$ is mainly related to effective precipitation and source $\delta^{18}O$ (Bar-Mathews et al., 2003; Verheyden et al., 2008; Grant et al., 2012; Nehme et al., 2015).

The general climate conditions of the penultimate glacial period in the central Levant

The isotope values of Kanaan stalagmite K2-2010 discontinuously cover the penultimate glacial period (Fig. 5).

https://doi.org/10.1017/qua.2018.18 Published online by Cambridge University Press

Overall, the Kanaan isotope record for MIS 6 exhibits a higher $\delta^{13}C$ and $\delta^{18}O$ variability (~4‰ for both) than the record for MIS 5 (Fig. 6) inferred from a stalagmite from the same cave (2.5‰ and 3‰, respectively) (Nehme et al., 2015) with infilling conditions, altitude, aspect, and distance from the sea that remained unchanged. The $\delta^{18}O$ values of the overall penultimate glacial period are comparable to values found after the glacial inception change from 120 to 84 ka (Nehme et al., 2015), invoking similar cold and drier climate conditions than the Eemian period. However, the climatic conditions of the penultimate glacial period were less severe than the full glacial conditions of the MIS 3/4 period in the Levant as seen in the Soreq-Peqiin isotopic record (Bar-Matthews, 2014). The period from ~160 to ~162 ka was, however, exceptionally dry and cold, with less negative $\delta^{18}O$ and $\delta^{13}C$ values (Fig. 6).

The first speleothem studies on MIS 6/7 from the Soreq, Peqiin, Tzavoa, and Ma'ale-Dragot Caves demonstrated that the penultimate glacial conditions in the eastern Mediterranean were unstable and relatively cold, but more humid than the last glacial MIS 3 (Ayalon et al., 2002; Bar-Matthews et al., 2003; Vaks et al., 2006). Consequently, conditions were sufficiently humid to maintain drip water flow in the epikarst zone, and temperatures warm enough to support the soil CO_2 concentration activity, leading to calcite precipitation in the cave during this glacial period. These findings contradict Cheddadi and Rossignol-Strick (1995), who argued that conditions in the eastern Mediterranean during early MIS 6 were very cold and arid, with precipitation below 200 mm, similar to the last two glacial maxima of MIS 4 and 2.

In the Kanaan speleothem, although $\delta^{18}O$ shows important changes during MIS 6 (Fig. 5), $\delta^{13}C$ does not exceed –9‰ (with exception of two short excursions to –8‰), reflecting the contribution of carbon from soil CO_2 derived from C3 type vegetation. Additionally, the regular changes in $\delta^{18}O$, speleothem diameter, and macroscopic aspect of the speleothem suggest the occurrence of climatic instabilities.

The climate conditions during the early penultimate glacial period (185–163 ka)

The basal part of the stalagmite covers discontinuously the early penultimate glacial period from 163 to 194 ka, with an arrangement of columnar and monocrystalline crystals, attributed by Frisia (2015) to a slow/very low drip rate (Fig. 5). This is in agreement with growth rates of up to ~1 mm/ka as suggested by Dreybrodt (1988). During the early penultimate glacial period, two long hiatuses have been detected from ~190 to ~183 ka and from ~175 to ~163 ka (Fig. 5). The second hiatus starts at a time of very negative $\delta^{18}O$ values and suggests either a sample-specific signal or a flooding period (Zhornyak et al., 2011) as the basal part of the speleothem grew on rimstone dams that cover the cave floor of this part of Kanaan Cave. Hiatuses for the same time frame were observed in the Peqiin speleothem record in the southern Levant, interpreted as reflecting a sampling bias rather than periods when speleothem growth actually ceased. However, no such hiatus is observed in the continuous Soreq record for the same period even though both records are controlled by the same eastern Mediterranean moisture source. Therefore, the occurrence of hiatuses in the Kanaan record precludes any regional significance for the growth interruption. Still, the mid–penultimate period is continuous in the Kanaan records and displays high variability in the isotope profile.

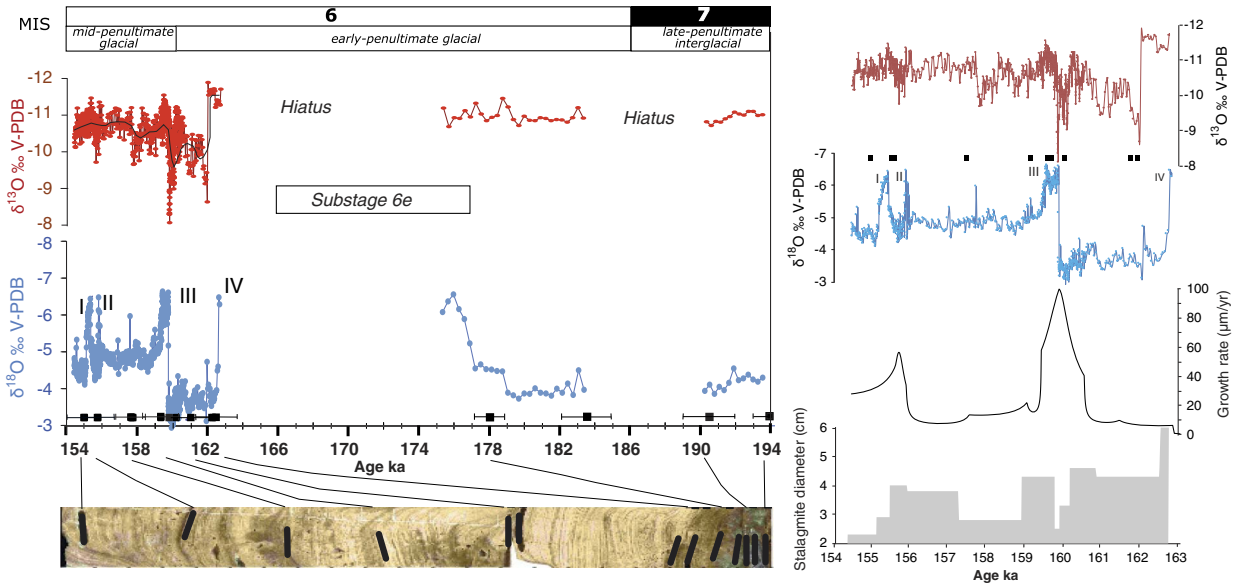

Figure 5. (color online) $\delta^{18}O$ and $\delta^{13}C$ profiles microdrilled along the growth axis of stalagmite K2-2010 (Kanaan Cave, Lebanon) reported with their radiometric age. The $\delta^{13}C$ data are presented with their moving average (black line) to clearly show the isotopic variations during the $\delta^{18}O$ peaks I, II, III, and IV. On the right, the isotopic changes from 154 to 163 ka are displayed together with growth rate and stalagmite diameter. V-PDB, Vienna Pee Dee belemnite.

https://doi.org/10.1017/qua.2018.18 Published online by Cambridge University Press

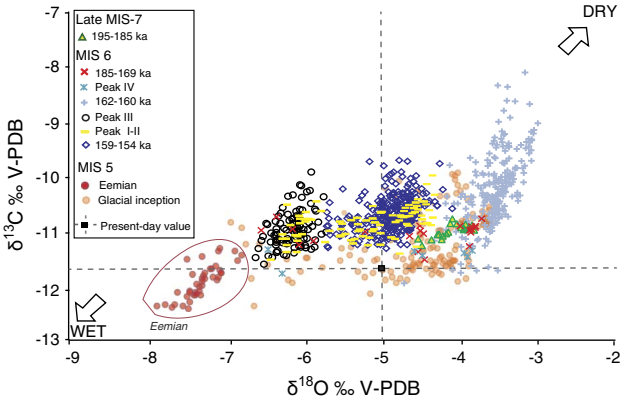

Figure 6. (color online) Cross plot of the stable isotope values from Kanaan Cave from late Marine Oxygen Isotope Stage (MIS) 7 to mid–MIS 6 (this study), MIS 5 (84–129 ka), and late Holocene (Nehme et al., 2015). The Eemian period recorded in Kanaan stalagmite lasted from 129 to 126 ka. The last glacial inception after ~120 ka is marked the beginning of a cooling period at the end of the Eemian period until the beginning of full glacial conditions of MIS 4. V-PDB, Vienna Pee Dee belemnite.

Overall, the basal part of the stalagmite suggests unfavorable conditions for speleothem deposition during the end of the penultimate interglacial period and the start of the penultimate glacial period. $\delta^{18}O$ values of approximately –4‰ (Fig. 5), previously interpreted as dry conditions (Verheyden et al., 2008; Nehme et al., 2015) during the MIS 5 period, are in agreement with Gasse et al., (2015) who showed that rather dense steppic vegetation around the Yammouneh paleolake reflect a dry and cold episode. By contrast, the $\delta^{13}C$ values of approximately –11‰, similar to last interglacial $\delta^{13}C$ values (Fig. 6), indicate a significant contribution of soil biogenic CO_2 and thus relatively humid (temperate to warm) conditions. Alternatively, low rainfall amounts sufficient to maintain an active soil and vegetation, but too low to sustain a regular effective recharge in the epikarst zone, might be a possible explanation for the observed stable isotope signatures versus growth rate.

Climatic dynamics during the mid–MIS 6 (163–154 ka)

An important change in speleothem growth rate and macroscopic form occurred around 163 ka. The upper part of the stalagmite shows growth rates ranging from 6 to 99 mm/ka. During the mid–penultimate glacial period (~163 to ~154 ka), $\delta^{18}O$ values are low (mean: –5.18‰) compared with the early penultimate (mean: –3.69‰), in agreement with a change toward more humid conditions, as also indicated by the increased growth rate (Fig. 5). The petrographic change from columnar monocrystalline in segment 1 to laminated structures in segments 2 and 3 (Fig. 4C, D, and E) reflects a significant hydrologic change within the epikarst. Layering in stalagmites consists of alternating dark and compact layers with whiter and more porous layers. This petrographic structure has been recorded in speleothems from high latitudes (Treble et al., 2005; Baldini et al., 2006; Verheyden et al., 2006; Van Rampelbergh et al., 2014) and tropical-subtropical sites (Shen et al., 2013; Breitenbach et al., 2015; Ridley et al., 2015). Such lamination is considered as indicative of seasonal changes in cave climate and chemistry (Proctor et al., 2000; Fairchild et al., 2001; Genty et al., 2001; Treble et al., 2005; Verheyden et al., 2006; Mattey et al., 2008; Van Rampelbergh et al., 2014) and in infiltration, which is related to the hydrologic functioning of the aquifer (Genty and Deflandre 1998; Fairchild et al., 2006; Verheyden et al., 2006; Van Rampelbergh et al., 2014; Breitenbach et al., 2015). The significance of such structures in a Mediterranean climate is very likely related to the Precipitation - Evaporation (P-E) balance, which determines the amount of effective precipitation (Bar-Matthews et al., 1996; Verheyden et al., 2008; Cheng et al., 2015) that could lead to higher seasonality with laminated structures in stalagmites (Ayalon et al., 2013).

From ~163 to ~155 ka, moderate to high growth rates infer a reactivation of water recharge (after the second, long hiatus). This growth rate change corresponds well with an alternation of white porous and dark compact layers (Fig. 4C and D). Although the layer couplets are very similar to seasonal layering as observed in other speleothems (Treble et al., 2005; Baldini et al., 2006; Verheyden et al., 2006; Van Rampelbergh et al., 2014), the seasonal character has yet to be confirmed.

Between 163 and 154 ka, oxygen and carbon isotopes evolve synchronously, although with higher amplitude variability in $\delta^{18}O$ values. This pattern is marked by several negative excursions in $\delta^{18}O$ values (Fig. 5) centered at ~155.3 ka (peak I), ~155.8 ka (peak II), ~159.7 (peak III), and ~162.7 ka (peak IV). The remarkable agreement between the evolution of growth rate, laminae fabric, and isotopic values (Fig. 5) supports a change in general conditions (i.e., rainfall, temperature, and/or soil conditions). As explained previously and based on earlier speleothem studies in the Levant, the changes in $\delta^{18}O$ most probably result from a change in source $\delta^{18}O$ and/or rainfall variations. It suggests short phases of wetter conditions during peaks I, II, III, and IV. High growth rates of 99 mm/ka for peak III and 58 mm/ka for peaks I and II are in agreement with higher rainfall amounts. These excursions lasted up to 500 yr and coincide with thicker dark compact laminae (Fig. 5), which might indicate excessive rainfall during a particular season, enough to maintain active infiltration conditions and calcite growth during the whole year. An alternative explanation of the low $\delta^{18}O$ values by only temperature changes is rather unlikely, as the observed changes of approximately 2‰ would require a change in temperature of 8°C to 10°C, which seems unreasonably high.

In the same section, the $\delta^{13}C$ values are fairly constant. However, two significant $\delta^{13}C$ excursions with less negative $\delta^{13}C$ values occur at 161.9 and 159.8 ka. Both coincide, within chronological uncertainties, with the stadial periods as defined in the Chinese Hulu-Sanbao record (Fig. 7B). The peak IV (~162.7 ka) with a noticeable negative shift in $\delta^{18}O$

https://doi.org/10.1017/qua.2018.18 Published online by Cambridge University Press

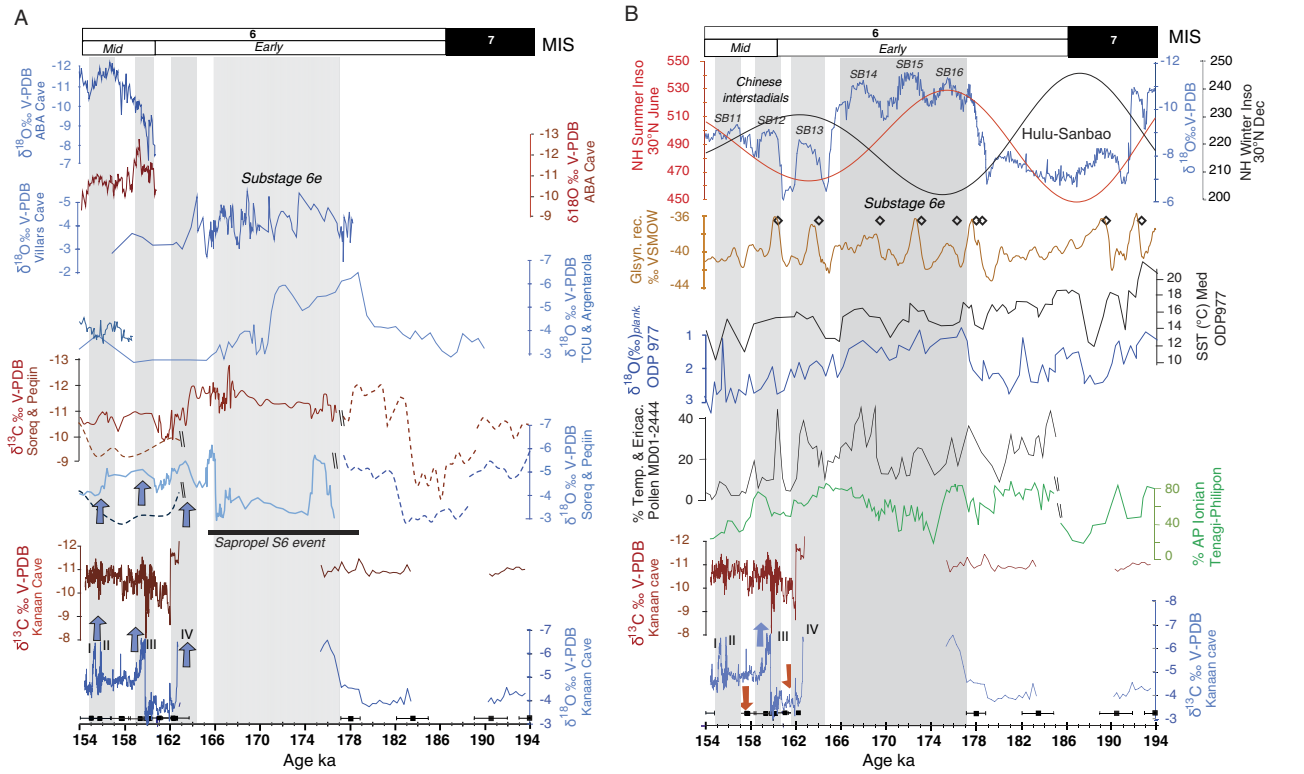

Figure 7. (color online) (A) Kanaan Cave $\delta^{18}O$ and $\delta^{13}C$ profiles compared with speleothem records in the Mediterranean basin. From bottom to the top: Soreq-Peqiin records (Ayalon et al., 2002; Bar-Mathews et al., 2003), Argentarola and Tana Che Urla (TCU) records in central and northern Italy (Bard et al., 2002; Regattieri et al., 2014), Villars Cave record in southern France (western Europe), and Abaliget (ABA) Cave records in southern Hungary (Koltai et al., 2017). (B) Kanaan Cave $\delta^{18}O$ and $\delta^{13}C$ profiles compared with continental and marine records in the Mediterranean and Northern Hemisphere. From bottom to the top: percent arboreal taxa records from the Ionian and Tenaghi-Philippon paleolakes (Tzedakis et al., 2004; Roucoux et al., 2008, 2011), percent temperate and Ericaceae taxa from the marine MD01-2444 core (Margari et al., 2014), $\delta^{18}O_{planktonic}$ records of the ODP 977 core (Martrat et al., 2004), sea surface temperature (SST) (°C) variations from ODP 977 (Martrat et al., 2004) in the western Mediterranean basin, the synthetic Greenland record (Barker et al., 2011) with the Dansgaard-Oeschger synthetic events (open diamonds), the Hulu-Sanbao speleothem (Wang et al., 2008), and the Northern Hemisphere (NH) insolation curve (Berger and Loutre, 1991). Gray shading indicates warming interstadial periods within the penultimate glacial period. Black squares indicate the age control points on the Kanaan isotope profile. Blue and red arrows highlight wet and dry periods, respectively. MIS, Marine Oxygen Isotope Stage; V-PDB, Vienna Pee Dee belemnite; VSMOW, Vienna standard mean ocean water.

coinciding with negative $\delta^{13}C$ values, combined with a slightly higher growth rate (6 mm/ka) than the basal part, suggests a short-lived wetter interval.

Millennial-scale oscillations during penultimate glacial MIS 6

Millennial- to submillennial-scale climate variability is clearly visible in the Kanaan record for 163 to 154 ka and with pronounced high-amplitude changes in the $\delta^{18}O$ profile. The $\delta^{18}O$ time series suggests at least three wetter phases (Fig. 7A) at ~155.3 ka (peak I), ~155.8 ka (peak II), ~159.7 (peak III), and ~162.7 ka (peak IV), in agreement with more negative $\delta^{13}C$ values and petrographic observations. These periods of low $\delta^{18}O$ and $\delta^{13}C$ values are interpreted as intervals of higher rainfall. This interpretation is in agreement with interstadial periods identified in the Hungarian Abaliget record (Koltai et al., 2017) and the Italian Tana Che Urla Cave record (Regattieri et al., 2014), as well as in Villars Cave, France (Wainer et al., 2013), and Soreq and Peqiin Caves in Israel (Ayalon et al., 2002).

The amplitude of the $\delta^{18}O$ peaks is 2‰ to 3‰. The $\delta^{18}O$ changes in the Kanaan records are slightly higher than the interstadial peaks identified in the Abaliget and Tana Che Urla records, with a 1.5‰ shift decrease in $\delta^{18}O$ from 150 to 155 ka. The negative $\delta^{18}O$ shifts in the Villars record reach an amplitude of up to 2‰ for the early MIS 6. In the Soreq-Peqiin record, $\delta^{18}O$ varies between 1‰ and 1.2‰ during mid–MIS 6 and up to 3‰ for early MIS 6. Indeed, Soreq Cave is located at 400 m asl in the southern Levant, with a lower rainfall gradient than the north Levant. The amplitudes of the $\delta^{18}O$ shifts in the Kanaan records are higher and are attributed to the cave's location at low elevation at 98 m asl, 1.2 km from the Mediterranean Sea, with higher rainfall amounts with isotopically heavier composition reaching the cave. The $\delta^{18}O$ change during the warm interstadial peaks most probably reflects a combined change in rainfall amount

https://doi.org/10.1017/qua.2018.18 Published online by Cambridge University Press

and seasonality, because large source changes as demonstrated for Soreq and Argentarola Caves during the S6 interval (Rossignol-Strick, 1995; Ayalon et al., 2002; Bard et al., 2002; Bar-Matthews et al., 2003; Emeis et al., 2003; Schmiedl et al., 2003) seem unlikely. Within the age uncertainties of the marine records, the $\delta^{18}O$ minima in Kanaan Cave correspond roughly with $\delta^{18}O_{plank.g.bul.}$ peaks (0.8‰ to 1.8‰ amplitude) observed in marine core ODP-977A from the western Mediterranean (Martrat et al., 2004), with an abrupt warming event recorded in the same core at ~156 ka and with warmer SST-U^{k}_{37} between ~158 and ~164 ka. These high SST values combined with $\delta^{18}O_{plank.}$, both indicating changes in the Mediterranean hydrologic budget, suggest a possible link with short global warming phases. In the eastern Mediterranean basin, SSTs were also not lower than 15°C (Emeis et al., 2003), suggesting that climatic conditions during mid–MIS 6 were certainly not those of an extreme glacial state. These related changes imply that even under glacial conditions, rainfall peaks in the Levant were predominantly governed by westerly cyclones bringing moisture from the Atlantic Ocean with sufficiently temperate SSTs to produce moisture over the Mediterranean Sea and precipitation over the Levantine coast.

According to the age model with decadal resolution (average: 11 yr) for the 163–154 ka period, these wet events lasted 0.64, 0.24, 0.5, and 0.2 ka, respectively. The time interval of the four peaks in the Kanaan record is short compared with the duration of the millennial-scale peaks (0.8 to 2.6 ka) in the Villars record for the early MIS 6. Also, the Abaliget (Hungary) and Tana Che Urla (Italy) speleothem records show an interstadial peak that lasted up to 2 ka (from 154 to 155 ka and from 151.6 to 154 ka, respectively). Within the limit of the age uncertainties, the wet peaks in the Kanaan record invoke a rapid and short response to regional wet pulses in the eastern Mediterranean similar to other European records.

The timing of the four wet $\delta^{18}O$ peaks (I–II, III, and IV) are consistent with the timing of smaller isotope excursions in the Peqiin-Soreq record, within the limit of age uncertainties of the Kanaan record (Fig. 7A). Peak I–II in Kanaan Cave coincides with the timing of the interstadial event in Abaliget Cave, Hungary, that lasted from 154 to 155 ka. All interstadial peaks in the Kanaan record coincide, in general, with the arboreal pollen variations in the Ionian (Roucoux et al., 2008, 2011) and Tenaghi-Philippon (Tzedakis et al., 2004) pollen profiles, despite their limited age control (Fig. 7B). Temperate coniferous forest expanded in a broadscale pattern from 185 to 155 ka in northern Greece (Roucoux et al., 2008). In northern Lebanon, the Yammouneh pollen curve (Gasse et al., 2015) shows widespread temperate deciduous forests (*Quercus*) during mid–MIS 6, while steppe taxa (*Artemisia* and Chenopodiaceae) are less significant during the mid–penultimate glacial period, reflecting a generally humid climate that supported elevated vegetation activity in the central Levant, with a more negative $\delta^{13}C$ signal. The temperate tree pollen curve from the Portuguese margin (Margari et al., 2010, 2014) and specifically the Ericaceae curve (Hodell et al., 2008, 2013) reveal millennial-scale variations within the same time frame of Kanaan interstadial peaks (Fig. 7B).

On a global scale, peaks III and IV agree with the timing of D-O-like events in the synthetic Greenland temperature record, GLT*syn* (Barker et al., 2011), suggesting a possible atmospheric teleconnection between the North Atlantic and the midlatitude Mediterranean region. Rapid changes of $\delta^{18}O$ values in peaks IV, III, II, and I closely track the Chinese SB11, 12, and 13 interstadial periods (Fig. 7B). The Kanaan record clearly shows a double peak (peaks II and I), with a return to drier conditions between both minima, only slightly visible in SB11 and not found in the GLT record (Wang et al., 2008; Cheng et al., 2016). Similarities do exist in the timing and structure of the Chinese interstadial periods recorded by Hulu Cave stalagmites and the Kanaan record for the period 154–163 ka. This underlines the intrahemispheric teleconnection between the North Atlantic region (including the Mediterranean basin) and the low- to midlatitudes of eastern Asia, which argues for an atmospheric link via the interaction between the westerlies and the subtropics (Cheng et al., 2012).

CONCLUSIONS

The stalagmite record K2-2010 from Kanaan Cave, Lebanon, provides a multiproxy (stable isotopes and petrography) record at a centennial resolution for the early MIS 6 (194–163 ka) in the eastern Mediterranean and a more highly resolved, multiproxy record in mid–MIS 6 (163–154 ka) that exhibits annual to decadal resolution. The well-constrained age model for the upper part of MIS 6 enables the correlation of climatic variability recorded in the synthetic Greenland and Chinese speleothem records. The main features of the K2-2010 record show the following.

The basal part of the Kanaan records covers discontinuously the early penultimate glacial period from 194 to 163 ka. During the end of the penultimate interglacial period and the start of the penultimate glacial period, the climatic conditions were unfavorable for speleothem deposition with low rainfall amounts sufficient to maintain an active soil and vegetation, but too low to sustain a regular effective recharge.

The mid–penultimate glacial period (~163 to ~154 ka) was characterized by wet conditions in the central Levant. The Kanaan speleothem shows higher growth rates and marked laminae, indicating increased water recharge of the epikarst. $\delta^{18}O$ and $\delta^{13}C$ values evolve coevally, with high-amplitude variations in $\delta^{18}O$ values, but relatively stable low $\delta^{13}C$ values during the mid–MIS 6. Several sudden negative $\delta^{18}O$ peaks (peaks I, II, III, and IV) concomitant with higher growth rates during each peak interval suggest intensified rainfall.

The negative $\delta^{18}O$ excursions during mid–MIS 6, combined with higher growth rates and low $\delta^{13}C$, can be associated with increased seasonal rainfall, similar to interstadial intervals. All wet periods (peaks I, II, III, and IV) show isotopic variations comparable with the Peqiin-Soreq and Abaliget speleothem records. The most striking

https://doi.org/10.1017/qua.2018.18 Published online by Cambridge University Press

similarity is the alignment of Kanaan peaks during the mid–penultimate glacial period with the D-O–like events observed in the GLT curve, indicating short interstadial periods in the central Levant. The Kanaan $\delta^{18}O$ peaks, occurring after the S6 sapropel event, infer a possible link between short regional wet phases in the Levant with global changes in surface and deep-water hydrography, as shown in the pollen records in the eastern and western Mediterranean basins and high-resolution marine records from the Iberian and Portuguese margins.

ACKNOWLEDGMENTS

This study was funded by the mobility fellowship program of the Belgian Federal Scientific Policy (BELSPO). The U.S. National Science Foundation funded Union College's isotope ratio mass spectrometer and peripherals (NSF-MRI #1229258). We acknowledge the assistance of the EDYTEM Laboratory (UMR-5204 CNRS) and Saint-Joseph University for making stalagmites from Kanaan Cave available for analyses during this study. We would like to thank the support of ALES (Association Libanaise d'Etudes Spéléologiques) members who accompanied us during field trips, as well as Kevin de Bondt and David Verstraten for laboratory analyses. S.R. Noble, A.R. Farrant, and D. Sahy publish with the approval of the executive director, British Geological Survey. We also thank the anonymous reviewers for their constructive comments and reviews.

REFERENCES

Ayalon, A., Bar-Matthews, M., Kaufman, A., 2002. Climatic conditions during marine isotopic stage 6 in the Eastern Mediterranean region as evident from the isotopic composition of speleothems: Soreq Cave, Israel. *Geology* 30, 303–306.

Ayalon, A., Bar-Matthews, M., Frumkin, A., Matthews, A., 2013. Last Glacial warm events on Mount Hermon: the southern extension of the Alpine karst range in the east Mediterranean. *Quaternary Science Reviews* 59, 43–56.

Baker, A., Genty, D., Dreybrodt, W., Barnes, W.L., Mockler, N.J., Grapes, J., 1998. Testing theoretically predicted stalagmite growth rate with Recent annually laminated samples implication for past stalagmite deposition. *Geochimica et Cosmochimica Acta* 62, 393–404.

Baker, A., Smart, P.L., 1995. Recent flowstone growth rates: field measurements in comparison to theoretical predictions. *Chemical Geology* 122, 121–128.

Baldini, J.U.L., McDermott, F., Fairchild, I.J., 2006. Spatial variability in cave dripwater hydrochemistry: implications for stalagmite paleoclimate records. *Chemical Geology* 235, 390–404.

Bard, E., Antonioli, F., Silenzi, S., 2002. Sea-level during the penultimate interglacial period based on a submerged stalagmite from Argentarola Cave (Italy). *Earth and Planetary Science Letters* 196, 135–146.

Barker, S., Diz, P., Vautravers, M.J., Pike, J., Knorr, G., Hall, I. R., Broecker, W.S., 2009. Interhemispheric Atlantic seesaw response during the last deglaciation. *Nature* 457, 1097.

Barker, S., Knorr, G., Edwards, R.L., Parrenin, F., Putnam, A.E., Skinner, L.C., Wolff, E., Ziegler, M., 2011. 800,000 years of abrupt climate variability. *Science* 334, 347–351.

Bar-Matthews, M., 2014. History of water in the Middle East and North Africa. In: Holland, H.D., Turekian, K.K. (Eds.), Treatise on Geochemistry. 2nd ed. Elsevier, Oxford, pp. 109–128.

Bar-Matthews, M., Ayalon, A., Gilmour, M., Matthews, M., Hawkesworth, C., 2003. Sea-land isotopic relationships from planktonic foraminifera and speleothems in the Eastern Mediterranean region and their implications for paleorainfall during interglacial interval. *Geochimica Cosmochimica Acta* 67, 3181–3199.

Bar-Matthews, M., Ayalon, A., Kaufman, A., Wasserburg, G.J., 1999. The Eastern Mediterranean paleoclimate as a reflection of regional events: Soreq Cave, Israel. *Earth and Planetary Science Letters* 166, 85–95.

Bar-Matthews, M., Ayalon, A., Matthews, A., Sass, E., Halicz, L., 1996. Carbon and oxygen isotope study of the active water-carbonate system in a karstic Mediterranean cave: implications for paleoclimate research in semiarid regions. *Geochimica et Cosmochimica Acta* 60, 337–347.

Berger, A., Loutre, M.F., 1991. Insolation values for the climate of the last 10 million years. *Quaternary Science Reviews* 10, 297–317.

Blunier, T., Brook, E.J., 2001. Timing of millennial-scale climate change in Antarctica and Greenland during the last glacial period. *Science* 291, 109–112.

Borsato, A., Quinif, Y., Bini, A., Dublyansky, Y., 2005. Open-system alpine speleothems: implications for U-series dating and paleoclimate reconstructions. Studi Trentini Di Scienze Naturali, Acta. *Geologica* 80, 71–83.

Breitenbach, S.F.M., Lechleitner, F.A., Meyer, H., Diengdoh, G., Mattey, D., Marwan, N., 2015. Cave ventilation and rainfall signals in dripwater in a monsoonal setting – a monitoring study from NE India. *Chemical Geology* 402, 111–124.

Breitenbach, S.F.M., Rehfeld, K., Goswami, B., Baldini, J.U.L., Ridley, H.E., Kennett, D.J., Prufer, K.M., et al., 2012. Constructing proxy records from age models (COPRA). *Climate of the Past* 8, 1765–1779.

Capron, E., Landais, A., Chappellaz, J., Schilt, A., Buiron, D., Dahl-Jensen, D., Johnsen, S.J., et al., 2010. Millennial and sub-millennial scale climatic variations recorded in polar ice cores over the last glacial period. *Climate of the Past* 6, 345–365.

Cheddadi, R., Rossignol-Strick, M., 1995. Eastern Mediterranean Quaternary paleoclimates from pollen and isotope records of marine cores in the Nile cone area. *Paleoceanography* 10, 291–300.

Cheng, H., Edwards, R.L., Sinha, A., Spötl, C., Yi, L., Chen, S., Kelly, M., Kathayat, G., Wang, X., Li, X., Kong, X., Wang, Y., Ning, Y., Zhang, H., 2016. The Asian monsoon over the past 640,000 years and ice age terminations. *Nature* 534, 640–646.

Cheng, H., Edwards, R.L., Shen, C.C., Polyak, V.J., Asmerom, Y., Woodhead, J., Hellstrom, J., et al., 2013. Improvements in 230 Th dating, 230 Th and 234 U half-life values, and U–Th isotopic measurements by multi-collector inductively coupled plasma mass spectrometry. *Earth and Planetary Science Letters* 371, 82–91.

Cheng, H., Sinhac, A., Verheyden, S., *et al.*, 2015. The climate variability in northern Levant over the past 20,000 years. *Geophysical Research Letters* 42, 8641–8650.

Cheng, H., Zhang, P.Z., Spötl, C., Edwards, R.L., Cai, Y.J., Zhang, D.Z., Sang, W.C., Tan, M., An, Z.S., 2012. The climatic cyclicity in semiarid-arid central Asia over the past 500,000 years. *Geophysical Research Letters* 39, L01705.

Dansgaard, W., 1964. Stable isotopes in precipitation. *Tellus* 16, 436–468.

https://doi.org/10.1017/qua.2018.18 Published online by Cambridge University Press

Dansgaard, W., Johnsen, S.J., Clausen, H.B., Dahl-Jensen, D., Gundestrup, N.S., Hammer, C.U., Hvidberg, C.S., et al., 1993. Evidence for general instability of past climate from a 250-kyr ice-core record. *Nature* 364, 218–220.

de Abreu, L., Shackleton, N., Schönfeld, J., Hall, M., Chapman, M., 2003. Millennial-scale oceanic climate variability off the Western Iberian margin during the last two glacial periods. *Marine Geology* 196, 1–20.

Dreybrodt, W., 1988. Processes in Karst Systems. Springer, New York.

Dreybrodt, W., 1999. Chemical kinetics, speleothem growth and climate. *Boreas* 28, 347–356.

Dubertret, L., 1975. Introduction à la carte géologique au 1/50000 du Liban. *Notes et Mémoires sur le Moyen-Orient* 23, 345–403.

Edwards, R.L., Chen, J.H., Ku, T.L., Wasserburg, G.J., 1987. Precise timing of the last interglacial period from mass spectrometric determination of ^{230}Th in corals. *Science* 236, 1547–1553.

Ehlers, J., Gibbard, P.L., 2007. The extent and chronology of Cenozoic global glaciation. *Quaternary International* 164, 6–20.

Ehlers, J., Grube, A., Stephan, H.-J., Wansa, S., 2011. Pleistocene glaciations of North Germany—new results. In: Ehlers, J., Gibbard, P.L., Hughes, P.D. (Eds.), Quaternary Glaciations – Extent and Chronology: A Closer Look. Developments in Quaternary Sciences 15. Elsevier, Amsterdam, pp. 149–162.

Emeis, K.C., Schulz, H., Struck, U., Rossignol-Strick, M., Erlenkeuser, H., Howell, M.W., Kroon, D., et al., 2003. Eastern Mediterranean surface water temperatures and ^{18}O during deposition of sapropels in the late Quaternary. *Paleoceanography* 18, 1005–1029.

Fairchild, I.J., Baker, A., 2012. Speleothem Science: From Processes to Past Environments. Quaternary Geosciences Series. Wiley-Blackwell, Chichester, UK.

Fairchild, I.J., Baker, A., Borsato, A., Frisia, S., Hinton, R.W., McDermott, F., Tooth, A.F., 2001. Annual to sub-annual resolution of multiple trace-element trends in speleothems. *Journal of the Geological Society* 158, 831–841.

Fairchild, I.J., Smith, C.L., Baker, A., Fuller, L., Spötl, C., Mattey, D., McDermott, F., 2006. Modification and preservation of environmental signals in speleothems. *Earth Science Reviews* 75, 105–153.

Fletcher, W.J., Goni, M.F.S., Allen, J.R., Cheddadi, R., Combourieu-Nebout, N., Huntley, B., Müller, U.C., 2010. Millennial-scale variability during the last glacial in vegetation records from Europe. *Quaternary Science Reviews* 29, 2839–2864.

Fletcher, W.J., Sánchez Goñi, M.F., 2008. Orbital- and sub-orbital-scale climate impacts on vegetation of the western Mediterranean basin over the last 48,000 yr. *Quaternary Research* 70, 451–464.

Fleitmann, D., Cheng, H., Badertscher, S., Edwards, R.L., Mudelsee, M., Göktürk, O.M., Fankhauser, A., et al., 2009. Timing and climatic impact of Greenland interstadials recorded in stalagmites from northern Turkey. *Geophysical Research Letters* 36, L19707.

Frisia, S., 2015. Microstratigraphic logging of calcite fabrics in speleothems as tool for paleoclimate studies. *International Journal of Speleology* 44, 1–16.

Frumkin, A., Ford, D. C., Schwarcz, H., 2000. Paleoclimate and vegetation of the Last Glacial cycles in Jerusalem from a speleothem record. *Global Biogeochemical Cycles* 14, 863–870.

Gasse, F., Vidal, L., Van Campo, E., Demory, F., Develle, A.-L., Tachikawa, K., Elias, A., et al., 2015. Hydroclimatic changes in northern Levant over the past 400 000 years. *Quaternary Science Reviews* 111, 1–8.

Genty, D., Baker, A., Vokal, B., 2001. Intra- and inter-annual growth rate of modern stalagmites. *Chemical Geology* 176, 191–212.

Genty, D., Blamart, D., Ghaleb, B., Plagnes, V., Causse, C., Bakalowicz, M., Zouari, K., et al., 2006. Timing and dynamics of the last deglaciation from European and North African δ^{13}C stalagmite profiles—comparison with Chinese and South Hemisphere stalagmites. *Quaternary Science Reviews* 25, 2118–2142.

Genty, D., Blamart, D., Ouahdi, R., Gilmour, M., 2003. Precise dating of Dansgaard–Oeschger climate oscillations in western Europe from stalagmite data. *Nature* 421, 833–837.

Genty, D., Deflandre, G., 1998. Drip flow variations under a stalactite of the Pere Noel cave (Belgium). Evidence of seasonal variations and air pressure constraints. *Journal of Hydrology* 211, 208–232.

Goñi, M.F.S., Turon, J.L., Eynaud, F., Gendreau, S., 2000. European climatic response to millennial-scale changes in the atmosphere–ocean system during the Last Glacial period. *Quaternary Research* 54, 394–403.

Grant, K.M., Rohling, E.J., Bar-Matthews, M., Ayalon, A., Medina-Elizalde, M., Bronk Ramsey, C., Satow, C., Roberts, A.P., 2012. Rapid coupling between ice volume and polar temperature over the past 150 kyr. *Nature* 491, 744–747.

Heiss, J., Condon, D.J., McLean, N., Noble, S.R., 2012. ^{238}U/^{235}U systematics in terrestrial uranium-bearing minerals. *Science* 335, 1610–1614.

Hellstrom, J., 2003. Rapid and accurate U/Th dating using parallel ion-counting multi-collector ICP-MS. *Journal of Analytical Atomic Spectrometry* 18, 1346–1351.

Hellstrom, J., 2006. U–Th dating of speleothems with high initial ^{230}Th using stratigraphical constraint. *Quaternary Geochronology* 1, 289–295.

Hendy, C.H., 1971. The isotopic geochemistry of speleothems—I. The calculation of the effects of different modes of formation on the isotopic composition of speleothems and their applicability as palaeoclimatic indicators. *Geochimica et Cosmochimica Acta* 35, 801–824.

Hodell, D.A., Channell, J.E.T., Curtis, J.H., Romero, O.E., Röhl, U., 2008. Onset of "Hudson Strait" Heinrich events in the eastern North Atlantic at the end of the Middle Pleistocene transition (~640 ka)? *Paleoceanography* 23, PA4218.

Hodell, D., Crowhurst, S., Skinner, L., Tzedakis, P.C., Margari, V., Maclaghlan, S., Rothwell, G., 2013. Response of Iberian Margin sediments to orbital and suborbital forcing over the past 420 kyr. *Paleoceanography* 28, 1–15.

Hoffmann, D.L., Spötl, C., Mangini, A., 2009. Micromill and in situ laser ablation sampling techniques for high spatial resolution MC-ICPMS U-Th dating of carbonates. *Chemical Geology* 259, 253–261.

Jouzel, J., Masson-Delmotte, V., Cattani, O., Dreyfus, G., Falourd, S., Hoffmann, G., Minster, B., et al., 2007. Orbital and millennial Antarctic climate variability over the past 800,000 years. *Science* 317, 793–796.

Koltai, G., Spötl, C., Shen, C.-C., Wu, C.-C., Rao, Z., Palcsu, L., Kele, S., Surányi, G., Bárány-Kevei, I., 2017. A penultimate glacial climate record from southern Hungary. *Journal of Quaternary Science* 32, 946–956.

Lachniet, M.S., Bernal, J.P., Asmerom, Y., Polyak, V., 2012. Uranium loss and aragonite–calcite age discordance in a calcitized aragonite stalagmite. *Quaternary Geochronology* 14, 26–37.

Litt, T., Pickarski, N., Heumann, G., Stockhecke, M., Tzedakis, P.C., 2014. A 600,000 year long continental pollen record from Lake

https://doi.org/10.1017/qua.2018.18 Published online by Cambridge University Press

Van, eastern Anatoloia (Turkey). *Quaternary Science Reviews* 104, 30–41.

Margari, V., Skinner, L.C., Hodell, D.A., Martrat, B., Toucanne, S., Grimalt, J.O., Gibbard, P.L., Lunkka, J.P., Tzedakis, P.C., 2014. Land-ocean changes on orbital and millennial time scales and the penultimate glaciation. *Geology* 42, 183–186.

Margari, V., Skinner, L.C., Tzedakis, P.C., Ganopolski, A., Vautravers, M., Shackleton, N.J., 2010. The nature of millennial-scale climate variability during the past two glacial periods. *Nature Geoscience* 3, 127–131.

Martrat, B., Grimalt, J.O., Lopez-Martinez, C., Chaco, I., Sierro, F.J., Flores, J.A., Zahn, R., Canals, M., Jason, H.C., Hodell, D.A., 2004. Abrupt temperature changes in the Western Mediterranean over the past 250,000 years. *Science* 306, 1762–1765.

Martrat, B., Grimalt, J.O., Shackleton, N.J., de Abreu, L., Hutterli, M.A., Stocker, T.F., 2007. Four climatic cycles of recurring deep and surface water destabilizations on the Iberian Margin. *Science* 317, 502–507.

Mattey, D., Lowry, D., Duffet, J., Fisher, R., Hodge, E., Frisia, S., 2008. A 53 year seasonally resolved oxygen and carbon isotope record from a modern Gibraltar speleothem: reconstructed drip water and relationship to local precipitation. *Earth and Planetary Science Letters* 269, 80–95.

Muñoz-García, M.B., Cruz, J., Martín-Chivelet, J., Ortega, A.I., Turrero, M.J., López-Elorza, M., 2016. Comparison of speleothem fabrics and microstratigraphic stacking patterns in calcite stalagmites as indicators of paleoenvironmental change. *Quaternary International* 407(Part A), 74–85.

Nehme, C., Verheyden, S., Noble, S.R., Farrant, A.R., Sahy, D., Hellstrom, J., Delannoy, J.J., Claeys, P., 2015. Reconstruction of MIS 5 climate in the central Levant using a stalagmite from Kanaan Cave, Lebanon. *Climate of the Past* 11, 1785–1799.

Nehme, C., Voisin, C., Mariscal, A., Gérard, P.-C., Cornou, C., Jabbour-Gédéon, B., Ahmaz, S., et al., 2013. The use of passive seismological imaging in speleogenetic studies: an example from Kanaan Cave, Lebanon. *International Journal of Speleology* 42, 97–108.

North Greenland Ice Core Project members. 2004. High-resolution climate record of Northern Hemisphere climate extending into the Last Interglacial period. *Nature* 431, 147–151.

Ortega, R., Maire, R., Devès, G., Quinif, Y., 2005. High resolution mapping of uranium and other trace elements in recrystallized aragonite–calcite speleothems from caves in the Pyrenees (France): implication for U-series dating. *Earth and Planetary Science Letters* 237, 911–923.

Past Interglacials Working Group of PAGES. 2016. Interglacials of the last 800,000 years. *Reviews of Geophysics* 54, 162–219.

Peel, M.C., Finlayson, B.L., McMahon, T.A., 2007. Updated world map of the Köppen-Geiger climate classification. *Hydrology and Earth System Sciences* 11, 1633–1644.

Peterson, L.C., Haug, G.H., Hughen, K.A., Röhl, U., 2000. Rapid changes in the hydrologic cycle of the tropical Atlantic during the last glacial. *Science* 290, 1947–1951.

Proctor, C.J., Baker, A., Barnes, W.L., Gilmour, M.A., 2000. A thousand year speleothem proxy record of North Atlantic climate from Scotland. *Climate Dynamics* 16, 815–820.

Rasmussen, S.O., Bigler, M., Blockley, S.P., Blunier, T., Buchardt, S.L., Clausen, H.B., Cvijanovic, I., et al., 2014. A stratigraphic framework for abrupt climatic changes during the Last Glacial period based on three synchronized Greenland ice-core records: refining and extending the INTIMATE event stratigraphy. *Quaternary Science Reviews* 106, 14–28.

Regattieri, E., Zanchetta, G., Drysdale, R.N., Isola, I., Hellstrom, J.C., Roncioni, A., 2014. A continuous stable isotope record from the penultimate glacial maximum to the Last Interglacial (159–121 ka) from Tana Che Urla Cave (Apuan Alps, central Italy). *Quaternary Research* 82, 450–461.

Richards, D.A., Dorale, J.A., 2003. Uranium-series chronology and environmental applications of speleothems. *Reviews in Mineralogy and Geochemistry* 52, 407–460.

Ridley, H.E., Asmerom, Y., Baldini, J.U., Breitenbach, S.F., Aquino, V.V., Prufer, K.M., Culleton, B.J., et al., 2015. Aerosol forcing of the position of the intertropical convergence zone since AD 1550. *Nature Geoscience* 8, 195–200.

Rohling, E., Mayewski, P., Challenor, P., 2003. On the timing and mechanism of millennial-scale climate variability during the last glacial cycle. *Climate Dynamics* 20, 257–267.

Rossignol-Strick, M., 1995. Sea-land correlation of pollen records in the eastern Mediterranean for the glacial-interglacial transition: biostratigraphy versus radiometric time-scale. *Quaternary Science Reviews* 14, 893–915.

Rossignol-Strick, M., Paterne, M., 1999. A synthetic pollen record of the eastern Mediterranean sapropels of the last 1 Ma: implications for the time-scale and formation of sapropels. *Marine Geology* 153, 221–237.

Roucoux, K.H., Tzedakis, P.C., Frogley, M.R., Lawson, I.T., Preece, R.C., 2008. Vegetation history of the marine isotope stage 7 interglacial complex at Ioannina, NW Greece. *Quaternary Science Reviews* 27, 1378–1395.

Roucoux, K.H., Tzedakis, P.C., Lawson, I.T., Margari, V., 2011. Vegetation history of the penultimate glacial period (marine isotope stage 6) at Ioannina, north-west Greece. *Journal of Quaternary Science* 26, 616–626.

Roy-Barman, M., Pons-Branchu, E., 2016. Improved U–Th dating of carbonates with high initial ^{230}Th using stratigraphical and coevality constraints. *Quaternary Geochronology* 32, 29–39.

Schmiedl, G., Mitschele, A., Beck, S., Emeis, K.C., Hemleben, C., Schulz, H., Sperling, M., Weldeab, S., 2003. Benthic foraminiferal record of ecosystem variability in the eastern Mediterranean Sea during times of sapropel S_5 and S_6 deposition. *Palaeogeography, Palaeoclimatology, Palaeoecology* 190, 139–164.

Schwarcz, H.P., 1989. Uranium series dating of Quaternary deposits. *Quaternary International* 1, 7–17.

Scrivner, A. E., Vance, D., Rohling, E. J., 2004. New neodymium isotope data quantify Nile involvement in Mediterranean anoxic episodes. *Geology* 32, 565–568.

Shen, C.C., Lin, K., Duan, W., Jiang, X., Partin, J.W., Edwards, R.L., Cheng, H., Tan, M., 2013. Testing the annual nature of speleothem banding. *Scientific Reports* 3, 2633.

Siddall, M., Rohling, E.J., Almogi-Labin, A., Hemleben, C., Meischner, D., Schmelzer, I., Smeed, D.A., 2003. Sea-level fluctuations during the last glacial cycle. *Nature* 423, 853–858.

Smith, A.C., Wynn, P.M., Barker, P.A., Leng, M.J., Noble, S.R., Wlodek, T., 2016. North Atlantic forcing of moisture delivery to Europe throughout the Holocene. *Scientific Reports* 6, 24745.

Stockhecke, M., Sturm, M., Brunner, I., Schmincke, H.-U., Sumita, M., Kipfer, R., Cukur, D., Kwiecien, O., Anselmetti, F.S., 2014. Sedimentary evolution and environmental history of Lake Van (Turkey) over the past 600 000 years. *Sedimentology* 61, 1830–1861.

Stocker, T.F., Johnsen, S.J., 2003. A minimum thermodynamic model for the bipolar seesaw. *Paleoceanography* 18, 1087.

Treble, P.C., Chappell, J., Shelley, J.M.G., 2005. Complex speleothem growth processes revealed by trace element mapping

https://doi.org/10.1017/qua.2018.18 Published online by Cambridge University Press

and scanning electron microscopy of annual layers. *Geochimica et Cosmochimica Acta* 69, 4855–4863.

Tzedakis, P.C., Pälike, H., Roucoux, K.H., de Abreu, L., 2009. Atmospheric methane, southern European vegetation and low-mid latitude links on orbital and millennial timescales. *Earth and Planetary Science Letters* 277, 307–317.

Tzedakis, P.C., Roucoux, K.H., de Abreu, L., Shackleton, N.J., 2004. The duration of forest stages in southern Europe and interglacial climate variability. *Science* 306, 2231–2235.

Ünal-İmer, E., Shulmeister, J., Zhao, J.X., Uysal, I.T., Feng, Y.X., Nguyen, A.D., Yüce, G., 2015. An 80 kyr-long continuous speleothem record from Dim Cave, SW Turkey with paleoclimatic implications for the Eastern Mediterranean. *Scientific Reports* 5, 13560.

Vaks, A., Bar-Matthews, M., Ayalon, A., Matthews, A., Frumkin, A., Dayan, U., Halicz, L., Almogi-Labin, A., Schilman, B., 2006. Paleoclimate and location of the border between Mediterranean climate region and the Saharo-Arabian desert as revealed by speleothems from the northern Negev Desert, Israel. *Earth Planetary Science Letters* 249, 384–399.

Van Geldern, R., Barth Johannes, A.C., 2012. Optimization of instrument setup and post-run corrections for oxygen and hydrogen stable isotope measurements of water by isotope ratio infrared spectroscopy (IRIS). Limnology Oceanography. *Methods* 10, 1024–1036.

Van Rampelbergh, M., Verheyden, S., Allan, M., Quinif, Y., Keppens, E., Claeys, P., 2014. Seasonal variations recorded in cave monitoring results and a 10 year monthly resolved speleothem $\delta^{18}O$ and $\delta^{13}C$ record from the Han-sur-Lesse cave, Belgium. *Climate of the Past* 10, 1821–1856.

Verheyden, S., Baele, J.M., Keppens, E., Genty, D., Cattani, O., Cheng, H., Lawrence, E., Zhang, H., Van Strijdonck, M., Quinif, Y., 2006. The Proserpine stalagmite (Han-Sur-Lesse Cave, Belgium): preliminary environmental interpretation of the last 1000 years as recorded in a layered speleothem. *Geologica Belgica* 9, 245–256.

Verheyden, S., Nader, F.H., Cheng, H.J., Edwards, L.R., Swennen, R., 2008. Paleoclimate reconstruction in the Levant region from the geochemistry of a Holocene stalagmite from the Jeita cave, Lebanon. *Quaternary Research* 70, 368–381.

Wainer, K., Genty, D., Blamart, D., Bar-Matthews, M., Quinif, Y., Plagnes, V., 2013. Millennial climatic instability during penultimate glacial period recorded on a south-western France speleothem. *Palaeogeography, Palaeoclimatology, Palaeoecology* 376, 122–131.

Wainer, K., Genty, D., Daeron, M., Bar-Matthews, M., Vonhof, H., Dublyansky, Y., Pons- Branchu, E., et al., 2011. Speleothem record of the last 180 ka in Villars cave (SW France): investigation of a large $\delta^{18}O$ shift between MIS6 and MIS5. *Quaternary Science Reviews* 30, 130–146.

Wang, Y.J., Cheng, H., Edwards, R.L., An, Z.S., Wu, J.Y., Shen, C.-C., Dorale, J.A., 2001. A high-resolution absolute-dated Late Pleistocene monsoon record from Hulu Cave, China. *Science* 294, 2345–2348.

Wang, Y.J., Cheng, H., Edwards, R.L., Kong, X.G., Shao, X., Chen, S., Wu, J.Y., Jiang, X.Y., Wang, X.F., An, Z.S., 2008. Millennial- and orbital-scale changes in the East Asian monsoon over the past 224,000 years. *Nature* 451, 1090–1093.

Wolff, E.W., Chappellaz, J., Blunier, T., Rasmussen, S.O., Svensson, A., 2010. Millennial-scale variability during the last glacial: the ice core record. *Quaternary Science Reviews* 29, 2828–2838.

The World Bank. 2003. Republic of Lebanon: Policy Note on Irrigation Sector Sustainability. Report No. 28766-LE. The World Bank, Water, Environment, Social, and Rural Development Group, Middle East and North Africa Region, Agriculture and Rural Development Department, Washington, DC.

Zhornyak, L.V., Zanchetta, G., Drysdale, R.N., Hellstrom, J.C., Isola, I., Regattieri, E., Piccini, L., Baneschi, I., Couchoud, I., 2011. Stratigraphic evidence for a "pluvial phase" between ca 8200–7100 ka from Renella cave (central Italy). *Quaternary Science Reviews* 30, 409–417.

Ziegler, M., Tuenter, E., Lourens, L.J., 2010. The precession phase of the boreal summer monsoon as viewed from the eastern Mediterranean (ODP Site 968). *Quaternary Science Reviews* 29, 1481–1490.

https://doi.org/10.1017/qua.2018.18 Published online by Cambridge University Press